Iron-carbide cluster thermal dynamics for catalyzed carbon nanotube growth

Feng Ding[a)]
Department of Experimental Physics, Göteborg University and Chalmers University of Technology, SE-412 96, Gothenburg, Sweden and Department of Physics, Qufu Normal University, Qufu 273165, People's Republic of China

Kim Bolton and Arne Rosén
Department of Experimental Physics, Göteborg University and Chalmers University of Technology, SE-412 96, Gothenburg, Sweden

(Received 23 October 2003; accepted 29 March 2004; published 20 July 2004)

Molecular dynamics simulations have been used to study the thermal behavior of $Fe_{N-m}C_m$ clusters where *N*, the total number of atoms, extends up to 2400. Comparison of the computed results with experimental data shows that the simulations yield the correct trends for the liquid–solid region of the iron-carbide phase diagram as well as the correct dependence of cluster melting point as a function of cluster size. The calculation indicates that, when carbon nanotubes (CNTs) are grown on large (>3–4 nm) catalyst particles at low temperatures (<1200 K), the catalyst particles are not completely molten. It is argued that the mechanism of CNT growth under these conditions may be governed by the surface melting of the cluster. © *2004 American Vacuum Society.*
[DOI: 10.1116/1.1752895]

I. INTRODUCTION

Transition metal clusters, such as iron, nickel, cobalt, and their alloys, are often used to grow CNTs.[1–3] For example, in the chemical vapor deposition (CVD) method, iron can be introduced as $Fe(CO)_5$,[4] as a layer of metal iron or as Fe clusters on a suitable substrate. At the elevated temperatures used for CNT growth (800–1500 K), it is believed that the $Fe(CO)_5$ or layer of deposited iron forms Fe clusters, and that these clusters catalyze nanotube growth. The size of the clusters, which together with other parameters such as the temperature and pressure determine the diameter and quality of the nanotubes, can be controlled by, for example, using deposited iron layers of varying thickness.[5]

The mechanism of catalyzed CNT growth is not well understood at the atomic level, and increased knowledge of this process, and the specific role of the metal cluster, may identify growth conditions where the structure (e.g., diameter and possibly chirality) can be precisely controlled. One of the models that have been proposed for CVD growth is the vapor–liquid–solid (VLS) model.[6–8] In this model the metal cluster has two distinct functions. First, the metal particles act as a catalyst to form C atoms from the reactants (e.g., methane or carbon monoxide). Second, the cluster acts as a solvent for these C atoms. Once the metal-carbide cluster (which is often thought to be in the liquid state) becomes supersaturated in carbon, and the cluster begins to cool, carbon atoms precipitate from the particle and form the carbon nanotube.

The mechanism of catalyzed CNT growth, at the atomic level, can be studied theoretically. Investigating the catalytic behavior of the metal catalyst requires an accurate description of the electron density and, if the growth dynamics is to be simulated, an accurate description of the time development of the electron density is required. Density functional theory (DFT) methods have been used for both static and dynamic calculations.[9–11] However, the computational expense of these methods severely restricts the length and number of trajectories that can be simulated, making chemical (statistically converged) analysis difficult.

Although a valid description of interatomic forces is also required when studying the role of the metal cluster as solvent, including the precise time development of the electron density is not expected to be as critical as when studying the cluster's catalytic role. Hence, when studying the role of the metal as a solvent, a valid analytic description of the metal–metal, metal–carbon, and carbon–carbon interactions should be sufficient to give qualitative and semiquantitative information of the metal–carbide cluster dynamics and subsequent CNT growth. An analytic force field will also allow for sufficiently long trajectories to be propagated, so that equilibrium thermal properties can be investigated.

In this contribution we present results of iron-carbide, FeC, cluster thermal dynamics obtained from molecular dynamics (MD) simulation based on an analytical potential energy surface. This surface gives the correct trends of the Fe–C phase diagram, which is expected to be important in studying dissolution and supersaturation of C in FeC particles. The potential energy surface also yields decreasing cluster melting point with decreasing cluster size, in excellent agreement with previous experimental and theoretical data for other metals. The agreement between the simulated and experimental data supports the validity of the dynamics obtained from this force field, and we use it to investigate trends in cluster thermodynamic properties and cluster melting mechanisms at the atomic level. The simulations indicate

[a)]Author to whom the correspondence should be addressed; electronic mail: fengding@fy.chalmers.se

that surface melting of FeC clusters is important for CNT growth at some of the temperatures typically used in CVD experiments. Other dynamical properties of FeC clusters, such as their coalescence, as well as SWNT nucleation from these clusters, will be presented in future contributions.

II. POTENTIAL ENERGY SURFACE AND SIMULATION METHODS

The many-body interaction potential, which is based on the second moment approximation of the tight binding model,[12] is suitable for studying the thermal properties of pure[13] and alloy[15] transition metal systems. The interaction energy between iron atoms is written as a sum of Born–Mayer-type repulsive and many-body attractive energy terms, i.e.,

$$E_{\mathrm{Fe-Fe}}=\sum_{i<j} A\exp\left[-p\left(\frac{r_{ij}}{r_0}-1\right)\right] - \left\{\sum_{i<j}\xi^2\exp\left[-2q\left(\frac{r_{ij}}{r_0}-1\right)\right]\right\}^{1/2}, \quad (1)$$

where r_{ij} is the distance between the ith and jth iron atoms. The constants $A=0.133\,15$ eV, $\xi=1.6179$ eV, $p=10.50$, $q=2.60$, and $r_0=2.553$ Å are obtained by fitting the cohesive energy, lattice parameter and elastic constants of $\gamma-$Fe(fcc structure).[14,15]

A valid description of the interaction between carbon and iron atoms is also important when simulating the iron-carbide system. The Johnson potential is known to be well suited for carbon in Fe, martensite and cementite.[16–19] According to the Johnson potential, the interaction energy between iron and carbon atoms is

$$E_{\mathrm{Fe-C}}=\sum_{i\neq j} -\epsilon\left[2\left(\frac{\frac{r_{ij}}{r_0}-\frac{r_c}{r_0}}{\frac{r_c}{r_0}-1}\right)^3-3\left(\frac{\frac{r_{ij}}{r_0}-\frac{r_c}{r_0}}{\frac{r_c}{r_0}-1}\right)^2\right] \times H(r_c-r), \quad (2)$$

where

$$H(x)=\begin{cases}1, & \text{if } x\geqslant 0\\ 0, & \text{if } x<0\end{cases}$$

is a step function that truncates the Fe–C interaction energy and r_{ij} is the distance between the ith iron and jth carbon atoms. The constants $\epsilon=0.35$ eV, $r_0=1.94$ Å, and $r_c=2.53$ Å are obtained by fitting the experimental data for α-Fe (the migration energy of carbon atoms, the activation volume of carbon migration, and the vacancy-carbon binding energy).[17]

Carbon is soluble in iron at low concentrations, and the carbon atoms do not aggregate until the system is supersaturated.[20] Under these conditions the attractive interaction between carbon atoms is very weak, and a purely repulsive Born–Mayer potential[21] has been proposed for the dissolved carbon–carbon interactions.[17,22] At high temperatures the stable phase of iron-carbide is Fe_3C, and when the mole fraction of carbon is larger than that of Fe_3C the system is supersaturated with carbon, which begins to aggregate. Under these (supersaturated) conditions the purely repulsive Born–Mayer potential is no longer valid.

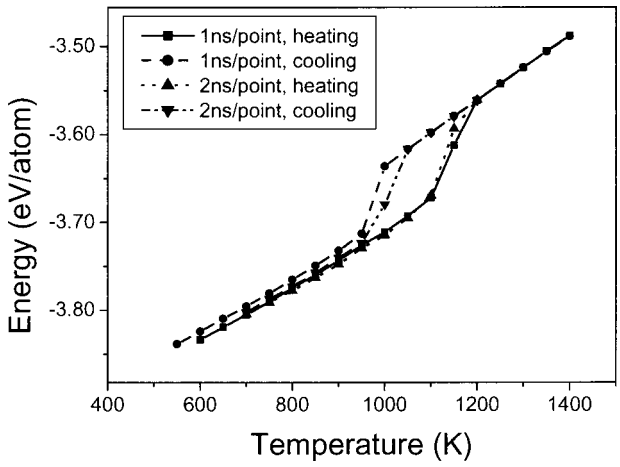

FIG. 1. Calorie lines for the Fe_{586} cluster obtained from MD simulations, where the cluster is heated and there are 5×10^5 (■) and 1×10^6 (▲) trajectory steps at each temperature, and the cluster is cooled and there are 5×10^5 (●) and 1×10^6 (▼) steps at each temperature. The time step is 2 fs.

Since iron-carbide clusters having a wide range of carbon concentrations, from pure iron to supersaturated systems, are studied here, both attractive and repulsive interactions are required for the C–C interactions. In this work these interactions are described by Lennard–Jones (L–J) potentials, with very weak attractive interactions. This L–J potential correctly identifies the existence of a stable Fe_3C phase and supersaturation of iron-carbide clusters with increasing carbon mole fraction. The total C–C interaction energy is the sum of all pair wise C–C L–J potentials, i.e.,

$$E_{\mathrm{C-C}}=\sum_{i<j} a(r_{ij})^{-12}-b(r_{ij})^{-6}, \quad (3)$$

where r_{ij} is the distance between ith and jth carbon atoms. The L–J parameters $a=34\,856.0$ eV/Å^{12} and $b=20.0$ eV/Å^6 are the same as those used previously for simulating the thermal properties of fullerene crystals.[23]

This potential energy surface was used in constant temperature molecular dynamics (MD) simulations to study the thermal properties of $Fe_{N-m}C_m$ nanoclusters, where m is the number of carbon atoms and N is the total number of the atoms in the cluster. In this work, cluster sizes of $55<N<2400$ (about 1–4 nm diameters) were studied, and the temperature ranged from 500 to 1400 K. These size and temperature ranges are similar to those found in CVD growth experiments.[4,5]

The integration time step was 2 fs, and 5×10^5 MD steps were propagated at each temperature. This is a sufficient number of steps to ensure the validity of the qualitative (and even semiquantitative) trends in cluster melting studied here. For example, Fig. 1 shows the calorie lines for the Fe_{586} cluster when heating and cooling this cluster from 600 and 1400 K, respectively. Comparison is made between calorie

lines obtained using 5×10^5 and 1×10^6 equilibration steps at each temperature. The first condition corresponds to a 1 ns trajectory for each temperature point in Fig. 1, and the second to 2 ns/point. Similar to the studies of Qi *et al.*,[24] we identify the melting point during the heating process as the temperature where the phase transition ends (i.e., at 1200 K from the 1 ns/point calorie line and 1150 K for the 2 ns/point line). The freezing point is identified as the temperature when the phase transition ends when cooling the cluster.[24] As seen in Fig. 1, the melting and freezing temperatures are not significantly changed when doubling the length of the trajectory, and hence the shorter integration time is used. Moreover, doubling the length of the simulation did not significantly reduce the hysteresis seen in the figure. That is, the calculation with 5×10^5 steps per temperature point yields a temperature gap between the freezing and melting points of about 250 K. Doubling the number of the steps per temperature point decreases the temperature gap by only 50 K.

Similar simulations to those discussed above for Fe_{586} were performed for the other clusters. When the calorie curve was obtained by cooling the cluster, the initial structure was generated by randomly placing the iron and carbon atoms in a sphere before thermalizing at the desired (liquid) temperature. When the calorie curve of pure iron clusters was obtained by heating, the initial structure was icosahedral (for $N=55$, 147, 309, 561, 923, 1415, and 2406) or Wulff polyhedral ($N=201$, 586, and 1289). Two of these clusters are shown in Fig. 2. These structures are very stable for transition metal clusters with sizes from several tens to several thousands of atoms.[25] This stability was also seen in our simulations, where no structural transitions were seen before the clusters melted. The initial structures of $Fe_{N-m}C_m$ clusters used in the heating simulations were obtained by randomly substituting m iron atoms with carbon atoms, and then relaxing to its local energy minimum.

During the simulation, the Lindemann index[26,27] of each atom and the whole cluster was calculated as

$$\delta_i=\frac{1}{N-1}\sum_{j(\neq i)}\frac{\sqrt{\langle r_{ij}^2\rangle_T-\langle r_{ij}\rangle_T^2}}{\langle r_{ij}\rangle_T},$$
$$\delta=\frac{1}{N}\sum_{i=1}\delta_i, \tag{4}$$

where δ_i and δ are the Lindemann index of atom i and the whole cluster, respectively, and $\langle\ldots\rangle_T$ denotes the thermal average. The melting point of bulk materials is often identified as the temperature where the Lindemann index exceeds 0.10.[27] However, the nanosize particles studied here do not have the sharp phase change temperature found for bulk materials since many atoms are located near the surface, and surface melting broadens the range where the phase transition occurs. Thus, in order to ensure that we calculate a melting temperature where most of the cluster has melted (i.e., the majority of atoms have large amplitude motion) we increase the criterion of the Lindemann index to 0.15. However, it should be noted that varying this value between 0.1 and 0.2 does not significantly affect the results presented here.

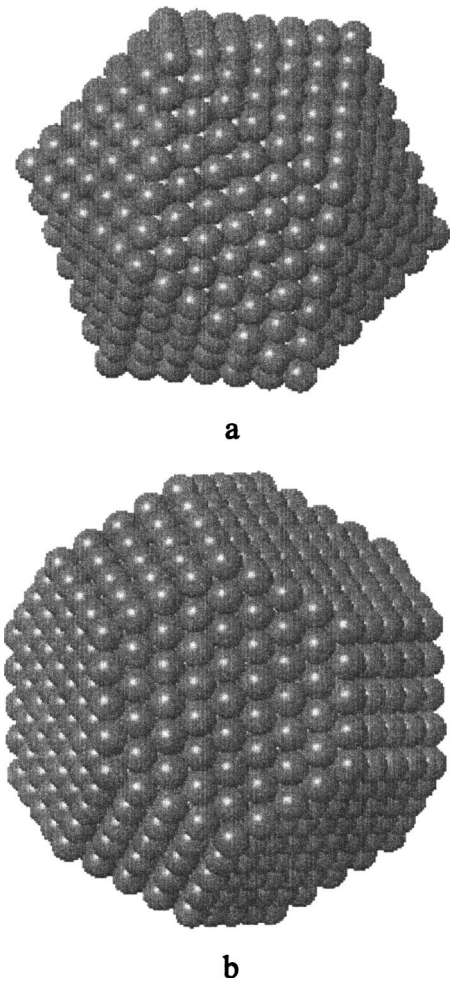

FIG. 2. Icosahedral structure of the Fe_{923} cluster (a) and Wulff-polyhedral structure of the Fe_{1289} cluster (b).

III. RESULTS AND DISCUSSION

A. Phase diagram of $Fe_{N-m}C_m$ clusters

The phase diagram of iron-carbide is very complex, with many solid phase structures.[28] The melting point of bulk FeC decreases from 1812 K for pure iron to 1403 K when the carbon content is 8.4% in number. After this eutectic point, the melting temperature increases and when the carbon content is 25.0% it is 1525 K. A simplified liquid–solid phase diagram of bulk iron-carbide, modified from the experimental phase diagram,[28] showing these features is given in the inset of Fig. 3. One important, very stable iron-carbide phase, Fe_3C, is found over the entire carbon content range after the eutectic point.[28] Iron carbides that have a carbon content larger than that of the Fe_3C phase are supersaturated in carbon. In this work, we study the melting point of $Fe_{N-m}C_m$ clusters with carbon contents ranging from 0% to 20%, and thereby obtain qualitative trends of the iron-carbide phase diagram relevant to CNT growth.

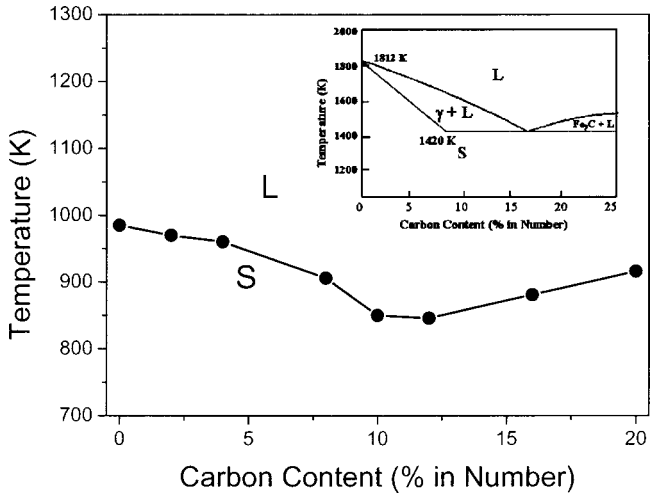

FIG. 3. Liquid–solid phase diagram of $Fe_{500-m}C_m$ clusters. The inset shows the associated phase diagram for bulk iron-carbide. The liquid phase is indicated by "L" and solid phase by "S."

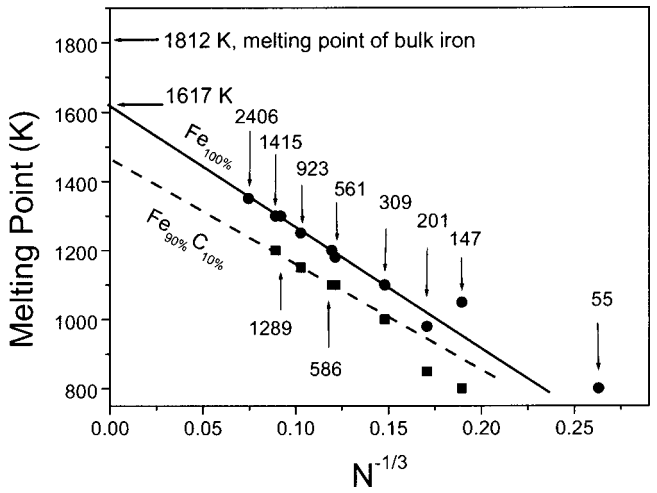

FIG. 4. Size dependence of Fe_N (●) and $Fe_{90\%}C_{10\%}$ (■) cluster melting points. The solid and dashed lines are linear fits to data for $N>300$.

As mentioned in the previous section, trends in cluster melting points can be obtained by cooling or heating the cluster through its phase transition. The difference in melting points obtained from these two approaches is less than 200 K. Trends in the $Fe_{N-m}C_m$ melting point with varying carbon contents can be obtained using either cooling or heating, although it is preferable to use the same approach for all calorie curves that are compared to each other (to avoid the hysteresis effect obtained in the simulations). We have calculated the melting points of $Fe_{N-m}C_m$ clusters by cooling the cluster from temperatures well above the melting point. The cooling process is preferred to heating for this calculation because it is difficult to identify the ground (minimum energy) states of all $Fe_{N-m}C_m$ clusters, which is required for the initial structures in the heating simulations. The initial structure is not as important for cooling simulations since one begins with the liquid phase and there are large changes in the cluster structure during the simulations.

The melting points calculated for $Fe_{N-m}C_m$ clusters, when $N=500$, were used to obtain the phase diagram in Fig. 3. The trends in this phase diagram are very similar to those of experimental bulk iron carbide. First, the melting point decreases to a minimum, located at a carbon content of 8.7% for the bulk alloy and 10%–12% for the $Fe_{500-m}C_m$ cluster and second, after this eutectic mixture the melting point increases with increasing carbon content. This increase in temperature is due to the existence of the stable Fe_3C phase. The similarity of the phase diagrams of $Fe_{500-m}C_m$ clusters and the bulk material supports the validity of the potential energy surface for studying qualitative (and semiquantitative) thermal properties of $Fe_{N-m}C_m$ clusters.

B. Size dependence of the cluster melting point

The melting point of iron clusters, Fe_N, and clusters with 10% carbon were calculated by simulating the phase transition when heating the clusters (the clusters studied here have well-defined low temperature structures). The size dependence of the melting point is shown in Fig. 4.

The experimental melting point of bulk iron is 1812 K (Ref. 28) whereas the temperature predicted by extrapolation of the fitted line in Fig. 4 is 1617 K. Although inaccuracies in the potential energy surface may affect the melting points predicted by simulations, the 200 K difference is primarily due to the fact that many of the cluster atoms are near the surface. Qi *et al.* studied the melting of Ni clusters with sizes up to 8000 atoms.[24] They found that the melting point of bulk Ni obtained from simulations using periodic boundary conditions is about 170 K higher than that extrapolated from the cluster melting points. Our results are in very good agreement with this. Also, the melting points of the $(Fe_{90\%}C_{10\%})_N$ clusters studied here are about 100–150 K lower than those corresponding to pure Fe_N clusters. This is consistent with the phase diagram shown in Fig. 3.

It is well known that surface melting plays a dominant role in the melting of nanometer size clusters.[29,30] At temperatures below the melting point, surface atoms can move significant lengths from their lattice positions (and at higher temperatures even diffuse from these positions) more easily than atoms in the center of the cluster. As more surface atoms leave their lattice positions the cluster surface loses its original symmetry which, in turn, makes it easier for other surface atoms to leave their lattice positions. This increasing large amplitude motion (and eventual diffusion) of atoms below the cluster melting point is known as surface melting.

There are several classical models that describe melting of nanosize particles based on interfacial tension between solid–gas or solid–liquid and liquid–gas phases: the homogeneous melting model with a liquid skin,[31] the liquid–skin melting model[32,33] and the liquid nucleation and growth model with an unstable liquid skin.[34,35] All models predict that the melting point of nanosize particles varies inversely with the particle diameter:

$$T_m(D) = T_{mB}\left[1 - \frac{4\alpha}{(\rho_s H D)}\right], \quad (5)$$

where T_m (T_{mB}) is the melting point of the particle (bulk material), D is the diameter of the particle, ρ_s is the density of the solid, H is the latent heat of fusion and α is a model-dependent parameter. Many experimental[36–38] and theoretical[24] studies have confirmed this inverse relationship. It may be noted that this equation can be derived even when a liquid skin is not assumed. Hence, agreement between experimental or simulation data and this inverse relationship is not sufficient evidence for surface melting. Direct observation of, for example, increased diffusion of surface atoms compared with bulk atoms, as seen in our simulations, is needed as evidence for a liquid-like layer.

It is evident from Fig. 4 that the inverse relationship given in Eq. (5) is applicable for clusters with more than 300 atoms.[39] In contrast, the melting points of clusters with $N < 300$ do not show a linear relationship with $N^{-1/3}$, and hence Eq. (5) is not applicable in this size range. In this equation the surface tension is assumed to be constant for a given material, whereas it can be considered to be dependent on the cluster structure for small clusters (i.e., two clusters with the same surface area but different structures can have different surface energies). This indicates that structural symmetry is also important for smaller clusters, and is supported by the fact that small closed-shell icosahedral clusters (such as Fe_{147}) can have higher melting points than Wulff polyhedral clusters (such as Fe_{201}) of similar size. Icosahedral clusters are types of multiply twinned particles,[25,40] with all of its 20 surfaces having the (1,1,1) fcc structure. The higher symmetry increases the stability of icosahedral clusters, and they thus have higher melting points than the Wulff polyhedral structures.

It is also evident from Fig. 4 that introducing carbon into the iron clusters lowers their melting points. The carbon atoms remove the symmetry of the corresponding pure iron clusters, thereby destabilizing the clusters and reducing their melting points. Similar, to the pure iron clusters, the melting point decreases linearly with $N^{-1/3}$ for larger clusters. However, in contrast to the Fe_N clusters, there is a monotonic increase in melting point with increasing cluster size even for small sizes. It is likely that this is also due to the lowering in cluster symmetry when carbon atoms are introduced into the cluster.

There are many theoretical and experimental studies concerning the size dependence of the melting point of nanosized clusters such as Au,[31,34,41] Ni,[24] Al,[42] Pb,[36] Sn,[37] and In.[43] All studies yield the same trend in melting point as given by Eq. (5) for clusters larger than several nanometers. As shown in Table I, the melting point of all of these materials decreases by less than 20% (or 10%) compared to the bulk when the cluster diameter is 5 nm (or 10 nm). The present work indicates that the melting point of pure Fe particles of 5 nm ($N \simeq 8000$) and 10 nm ($N \simeq 60\,000$) is about 10% and 5% lower than that of bulk iron, whereas $Fe_{90\%}C_{10\%}$ particles of 5 and 10 nm have melting points that are about 9% and 4% lower than that of the bulk material, respectively. Thus, the decrease in melting point of Fe and $Fe_{90\%}C_{10\%}$ with decreasing cluster size is similar to that of the other metals.

TABLE I. Relative melting points of some clusters with sizes of 5 and 10 nm. T_m is the melting point and T_{mB} is the melting point of the corresponding bulk.

Material	5 nm $(T_{mB}-T_m/T_{mB})$	10 nm $(T_{mB}-T_m/T_{mB})$	Reference
Au	0.18	0.08	31
Al	0.08	0.04	42
Ni	0.15	0.07	24
Pb	0.12	0.06	36
Sn	0.20	0.10	37
Ag	0.02	0.01	43
Fe	0.10	0.05	Present work
$Fe_{90\%}C_{10\%}$	0.09	0.04	Present work

C. Metal carbide clusters for carbon nanotube growth

As discussed in Sec. I, the results presented here focus on the role of iron clusters as solvents for carbon atoms, e.g., prior to carbon nanotube growth. The qualitative and semiquantitiative trends of the thermal properties of these clusters in the temperature range relevant to nanotube growth have been studied. The melting points shown in Fig. 4 suggest that, especially for larger clusters ($D > 3-4$ or $N > 1000-2000$ nm), the iron-carbide cluster may not be completely molten at lower CNT growth temperatures (near 1200 K). Under these conditions surface diffusion and/or melting may be important for carbon nanotube nucleation and growth, where the surface layer has a similar function to the completely molten clusters at higher temperatures. That is, C atoms can diffuse in this layer (which thickens with increasing carbon content), and growth occurs once this layer becomes supersaturated in carbon. Results of our investigations of the CNT nucleation and growth process will be presented in a subsequent contribution.

IV. CONCLUSION

Molecular dynamics simulations based on an analytic potential energy surface have been used to study the thermal properties of iron-carbide nanoparticles. The work focuses on the role of iron as a solvent for carbon atoms in the temperature range relevant for CVD carbon nanotube growth. The simulations yield trends in the FeC phase diagram that agree with experimental data for the bulk material. In addition, the simulations yield the correct cluster size dependence of the melting point. This indicates that the potential energy surface and simulation method yield valid (semiquantitative) thermal equilibrium data, and provide a correct description of the surface melting process of iron-carbide clusters at temperatures relevant to CVD growth of carbon nanotubes. For example, the simulations reveal that the melting point of 5 nm iron-carbide particles is about 10% less than that of the corresponding bulk material. Since the eutectic melting temperature of iron-carbide is 1400 K, this suggests that the iron-carbide clusters may not be completely

molten in many CVD experiments of carbon nanotube growth. At these lower temperatures (<1200 K) nanotubes may grow from a solid particle or from the molten surface layer of a partially molten particle that, as seen in the simulations, can appear several hundreds of degrees below the bulk melting point.

ACKNOWLEDGMENTS

This work is funded by the Swedish Research Council and the Swedish Foundation for Strategic Research (The CARAMEL Consortium). We are also grateful to the Swedish National Allocations Committee for High Performance Computing for the allocated computer time at the national supercomputing facilities.

[1]*Carbon Nanotubes: Synthesis, Structure, Properties and Application*, edited by M. S. Dresselhaus, G. Dresselhaus, and Ph. Avouris (Springer, Berlin, 2001).
[2]H. Dai, Surf. Sci. **500**, 218 (2002).
[3]A. A. Puretzky, D. B. Geohegan, X. Fan, and S. J. Pennycook, Appl. Phys. A: Mater. Sci. Process. **70**, 153 (2000).
[4]K. Bladh, L. K. L. Falk, and F. Rohmund, Appl. Phys. A: Mater. Sci. Process. **70**, 317 (2000).
[5]J. I. Sohn, C.-J. Choi, S. Lee, and T.-Y. Seong, Jpn. J. Appl. Phys., Part 1 **41**, 4731 (2002).
[6]T. Nozaki, Y. Kimura, and K. Okazaki, J. Phys. D **35**, 2779 (2002).
[7]J. Gavillet, A. Loiseau, C. Journet, F. Willaime, F. Ducastelle, and J.-C. Charlier, Phys. Rev. Lett. **87**, 275504 (2001).
[8]G. Y. Zhang, X. C. Ma, D. Y. Zhong, and E. G. Wanga, J. Appl. Phys. **91**, 9324 (2002).
[9]X. Blase, J.-C. Charlier, A. De Vita, and R. Car, Phys. Rev. Lett. **84**, 5078 (1999).
[10]E. Hernandez, C. Goze, P. Bernier, and A. Rubio, Appl. Phys. A: Mater. Sci. Process. **68**, 287 (1999).
[11]D. Srivastava and S. N. Atluri, CMES **3**, 531 (2002).
[12]V. Rosato, M. Guillope, and B. Legrand, Philos. Mag. A **59**, 321 (1989).
[13]L. J. Lewis, P. Jensen, and J.-L. Barrat, Phys. Rev. B **56**, 2248 (1997).
[14]M. Guillope and B. Legrand, Surf. Sci. **215**, 577 (1989).
[15]J. Stanek, G. Marest, H. Jaffrezic, and H. Binczycka, Phys. Rev. B **52**, 8414 (1995).
[16]J. R. Beeler, J. Adv. Mater. Res. **4**, 295 (1970).
[17]A. V. Evteev, A. T. Kosilov, and A. V. Milenin, Phys. Status Solidi **43**, 2284 (2001).
[18]R. Yamamoto, H. Matsuoka, and M. Doyama, Phys. Status Solidi A **45**, 305 (1978).
[19]R. A. Johnson, Phys. Rev. A **134**, 1329 (1964).
[20]O. I. Ostrovskii, V. A. Grigoryan, and A. F. Visharev, *Svoystva Metallitcheskih Rasplavov* (Metallurgiya, Moscow, 1988), p. 304.
[21]W. Eckstein, *Computer Simulation of Iron-Solid Interactions* (Springer, Berlin, 1991).
[22]H. H. Anderson and P. Sigmund, Nucl. Instrum. Methods **38**, 238 (1965).
[23]L. A. Girifalco, J. Chem. Phys. **96**, 858 (1992).
[24]Y. Qi, T. Cagin, W. L. Johnson, and W. A. Goddard, J. Chem. Phys. **115**, 385 (2001).
[25]S. Ino, J. Phys. Soc. Jpn. **27**, 941 (1969).
[26]R. S. Berry, T. L. Beck, H. L. Davis, and J. Jellinek, Adv. Chem. Phys. **70**, 75 (1988).
[27]F. A. Lindemann, Phys. Z. **11**, 609 (1910).
[28]*Materials Science and Engineering: An Introduction*, 5th ed., edited by W. Callister (Wiley, New York, 1999).
[29]K. F. Peters, Y.-W. Chung, and J. B. Cohen, Appl. Phys. Lett. **71**, 2391 (1997).
[30]Y. J. Lee, E. K. Lee, and S. Kim, Phys. Rev. Lett. **86**, 999 (2001).
[31]P. A. Buffat and J. P. Borel, Phys. Rev. A **13**, 2287 (1976).
[32]C. R. M. Wronski, J. Appl. Phys. **18**, 1731 (1967).
[33]K. J. Hanszen, Z. Phys. **157**, 523 (1960).
[34]R. R. Vanfleet and J. M. Mochel, Surf. Sci. **341**, 40 (1995).
[35]H. Reiss, P. Mirabel, and R. L. Wetten, J. Phys. Chem. **92**, 7241 (1988).
[36]K. F. Peters, J. B. Cohen, and Y. W. Chung, Phys. Rev. B **57**, 13430 (1998).
[37]S. L. Lai, J. Y. Guo, V. Petrova, G. Ramanath, and L. H. Allen, Phys. Rev. Lett. **77**, 99 (1996).
[38]A. N. Goldstein, C. M. Echer, and A. P. Alivisatos, Science **256**, 1425 (1992).
[39]Assuming that all Fe (and $Fe_{90\%}C_{10\%}$) clusters have the same density, ρ_s, then $N=4\pi/3(D/2)^3\rho_s$ and hence, from Eq. (5), $T_m(D)-T_{mB}\propto N^{-1/3}$.
[40]F. Ding, H. Li, J. Wang, W. Shen, and G. Wang, Int. J. Mod. Phys. B **15**, 1947 (2001).
[41]H. B. Liu, J. A. Ascencio, M. P. Alvarez, and M. J. Yacaman, Surf. Sci. **491**, 88 (2001).
[42]S. L. Lai, J. R. A. Carlsson, and L. H. Allen, Appl. Phys. Lett. **72**, 1098 (1998).
[43]M. Dipple, A. Maier, V. Gimple, H. Wider, W. E. Evenson, R. L. Rasera, and G. Schatz, Phys. Rev. Lett. **87**, 095505 (2001).